Matter and Radiation at Extremes

RESEARCH ARTICLE

pubs.aip.org/aip/mre

Suppressing stimulated Raman side-scattering with vector light

Cite as: Matter Radiat. Extremes 8, 055603 (2023); doi: 10.1063/5.0157811
Submitted: 11 May 2023 • Accepted: 24 July 2023 •
Published Online: 11 August 2023

Xiaobao Jia,[1] Qing Jia,[1,a)] Rui Yan,[2,3] and Jian Zheng[1,3,a)]

AFFILIATIONS

[1] Department of Plasma Physics and Fusion Engineering and CAS Key Laboratory of Geospace Environment, University of Science and Technology of China, Hefei, Anhui 230026, China
[2] Department of Modern Mechanics, University of Science and Technology of China, Hefei 230026, China
[3] Collaborative Innovation Center of IFSA, Shanghai Jiao Tong University, Shanghai 200240, China

[a)] **Authors to whom correspondence should be addressed:** qjia@ustc.edu.cn and jzheng@ustc.edu.cn

ABSTRACT

Recent observations of stimulated Raman side-scattering (SRSS) in different laser inertial confinement fusion ignition schemes have revealed that there is an underlying risk of SRSS on ignition. In this paper, we propose a method that uses the nonuniform nature of the polarization of vector light to suppress SRSS, and we give an additional threshold condition determined by the parameters of the vector light. For SRSS at 90°, where the scattered electromagnetic wave travels perpendicular to the density profile, the variation in polarization of the pump will change the wave vector of the scattered light, thereby reducing the growth length and preventing the scattered electromagnetic wave from growing. This suppression scheme is verified through three-dimensional particle-in-cell simulations. Our illustrative simulation results demonstrate that for linearly polarized Gaussian light, there is a strong SRSS signal in the 90° direction, whereas for vector light, there is very little SRSS signal, even when the conditions significantly exceed the threshold for SRSS. We also discuss the impact of vector light on stimulated Raman backscattering, collective stimulated Brillouin scattering and two-plasmon decay.

I. INTRODUCTION

Laser inertial confinement fusion (ICF) exhibits rich laser–plasma instabilities (LPIs), such as stimulated Raman scattering (SRS),[1,2] stimulated Brillouin scattering (SBS),[1,2] two-plasmon decay (TPD),[3] and crossed-beam energy transfer (CBET),[4,5] along with other secondary instabilities. SRS, in which the incident electromagnetic wave is scattered by an electron plasma wave (EPW), has been the focus of attention for several decades; it reduces laser energy coupling efficiency and preheats the target capsule with hot electrons. Depending on the direction of the wave vector of the scattered light, SRS can be categorized as forward scattering, backward scattering, or side-scattering.

SRS exhibits absolute growth (temporal amplification of the initial seed) in a uniform plasma while experiencing convective growth (spatiotemporal amplification of the initial seed) in a nonuniform plasma except at a density of $0.25n_c$, where n_c is the critical density. In a nonuniform plasma, stimulated Raman side-scattering (SRSS) is thought to be absolute mode and hence is of great significance, since the scattered light tangential to the density gradient is scarcely affected by the inhomogeneity of the plasma. However, despite being performed under conditions far beyond the threshold for triggering the absolute mode, experiments in the twentieth century found little evidence for SRSS. Mostrom and Kaufman[6] clarified the discrepancy between theory and experiments, pointing out that SRSS undergoes transverse convective growth and can only enter the absolute growth stage after the saturation of the convective mode, and the finite width of the laser beam raises the threshold for detecting the absolute mode of SRSS.[6,7] After the 1980s, little attention was paid to SRSS in either experimental or theoretical investigations.

Recently, however, there has been renewed interest in SRSS as experimental results have demonstrated the crucial role that it plays in indirect-drive,[8,9] direct-drive,[10] and shock ignition[11] ICF ignition schemes. Collective SRSS via shared EPW has been suggested as a mechanism of hot electron generation in indirect-drive experiments

at the National Ignition Facility (NIF),[8,9] and collective SRSS via shared scattered light has been observed in a direct-drive experiment performed on the Omega facility.[12] Direct-drive experiments with a planar target at the NIF have shown SRSS to be the main contributor to hot electron generation under ignition-scale conditions.[13,14] Also, the importance of SRSS has been verified in shock ignition experiments at low densities.[15] Very recently, the dominance of SRSS over stimulated Raman backscattering (SRBS) has been identified at the SG-II UP facility[16] in double cone ignition[17] experiments. To control the hot electrons generated by SRSS, it is necessary to mitigate SRSS.

In this paper, we propose suppressing SRSS by vector light[18,19] featuring transversely varying polarization. The vector light is typically generated in two ways: as output from a specially designed or modified laser resonator or by using a spatial light modulator to manipulate the amplitude, phase, or both of two orthogonally linearly polarized lights (or two left- and right-handed circularly polarized lights).[20,21] The mechanism responsible for suppression of polarization distribution in the cross-section of the pump beam in SRSS has two aspects. First, in the initial stage, the maximum growth occurs when the polarization of the seed aligns with the pump, i.e., $\mathbf{E}_{\text{pump}} \| \mathbf{E}_{\text{seed}}$. Additionally, the direction of the scattered wave vector is perpendicular to the density gradient as well as the electric field of the seed, i.e., $\mathbf{k}_{\text{seed}} \parallel [\nabla n \times \mathbf{E}_{\text{seed}} (\mathbf{E}_{\text{pump}})]$. This implies that the scattered wave vector changes with the varying polarization of the pump. Consequently, the scattered seeds excited at different transverse locations become incoherent owing to the varying polarizations and changing wave vectors, which slows down the growth. Second, the variation in polarization will cause the convective growth process to cease. The scattered light convects with the group velocity in the direction of the wave vector, and the changes in the directions of the wave vector and group velocity reduce the convective length so that the convective gain decreases. As pointed out by Mostrom and Kaufman,[6] limited to the initial amplitude of the seed, the SRSS exhibits convective growth first and then absolute growth only if the convective gain is large enough. For vector light, the inhibited convective growth will prevent the scattered light from entering the absolute growth stage. Consequently, SRSS can be strongly suppressed.

Several LPI mitigation schemes have been proposed, such as the use of broadband light[22] or multicolor light,[23] sunlight-like lasers,[24] polarization smoothing[25] or smoothing by spectral dispersion,[26] and rotation of the polarization of the incident light.[27] These methods suppress SRSS by controlling the frequency spectrum, phase distribution, or light intensity, or by imposing a temporal change on the uniform polarization of the pump laser. In addition to these methods, other specific strategies for suppressing SRSS involve lowering the overlapping intensity,[8] adjusting the polarization arrangement of the beam,[8] utilizing a silicon ablator to increase the threshold,[13] reducing the spot size,[12] or modifying the laser pulse shape and hohlraum plasma conditions.[9] In this work, for the first time (to the best of our knowledge), we propose a scheme to inhibit LPIs using the nonuniform nature of the polarization of the vector light and present a parametric design of the vector light to suppress SRSS. As we will show by three-dimensional (3D) particle-in-cell (PIC) simulations, SRSS does not occur even when the conditions far exceed the threshold. The nonuniform polarization of the vector light provides additional avenues for exploring laser–plasma interaction. The remainder of the paper is organized as follows. In Sec. II, we present a verification via PIC simulation of the efficacy of vector light in suppressing SRSS. In Sec. III, we derive an additional threshold determined by the characteristic length of the vector light. In Sec. IV, we discuss the impact of vector light on backscattering, collective SBS, and TPD, and then summarize our work.

II. SIMULATIONS

The verification of the suppressive effect of vector light on SRSS is performed using the 3D PIC code EPOCH.[28] In this section, we describe one of the methods for the construction of vector light in this PIC code and then present contrasting simulation cases of vector light and linearly polarized Gaussian light to illustrate the suppressive effect on SRSS of vector light.

A. Construction of vector light in PIC code

We consider linearly polarized Gaussian light (case 1) and vector light (case 2), both having the same wavelength, beam waist, and maximum intensity. In case 1, the long pump pulse features a Gaussian intensity profile with a wavelength $\lambda_0 = 1\ \mu$m, a waist $w_0 = 10.875\lambda_0$, and a maximum intensity $I_0 = 4 \times 10^{15}$ W/cm^2, propagating along the z direction and polarized in the x direction. In the PIC code, the vector light is constructed by coherent superposition of two beams with orthogonal polarization[29] and different phase distributions. In case 2, Gaussian light polarized in the x direction with beam waist $w_1 = 5\lambda_0$ and Laguerre–Gaussian light[30] polarized in the y direction with waist $w_2 = 6.7\lambda_0$ and two indices $l = 1, p = 0$ are coherently superposed to give an equivalent beam waist $w_0 = 10.875\lambda_0$. The superposed electric field $\mathbf{E}$ in cylindrical coordinates reads

$$\mathbf{E} = 2\exp\left(-\frac{r^2}{w_1^2}\right)\hat{\mathbf{e}}_x + 1.5\left(\frac{2e}{|l|}\right)^{|l|/2}\left(\frac{r}{w_2}\right)^{|l|}\exp\left(-\frac{r^2}{w_2^2}\right)\exp(il\phi)\hat{\mathbf{e}}_y, \tag{1}$$

where $e \approx 2.718$ is the base of natural logarithms. The intensity and polarization distributions of the vector light are illustrated in Fig. 1. Notably, the vector light exhibits a nearly Gaussian intensity distribution, and the intensity distribution in cases 1 and 2 are nearly the same, as can be seen in Fig. 7 in the Appendix. To account for the degree of nonuniform polarization of the vector light, the characteristic length of variation of the polarization, L_p, which is the distance from the position of purely x-polarized to that of purely y-polarized light (or vice versa) in the cross-section of the vector light, is adopted. Owing to the high cost of 3D PIC simulations, the L_p in our simulation setups shown in Fig. 2 is about ten wavelengths. In practice, the magnitude of L_p can be determined by the method outlined in Sec. I.

B. Simulation setup

To isolate the effect of nonuniform polarization of vector light on SRSS and exclude competition[31] or transition[32] between different LPI processes, the physical parameters have been chosen as follows. The transversely uniform hydrogen plasma density varies from $0.19n_c$ ($z = 0\ \mu$m) to $0.235n_c$ ($z = 38\ \mu$m) along the z direction, corresponding to a density scale length of $L_n \approx 180\ \mu$m. The electron temperature is 500 eV, and the ion temperature is 100 eV. The ions

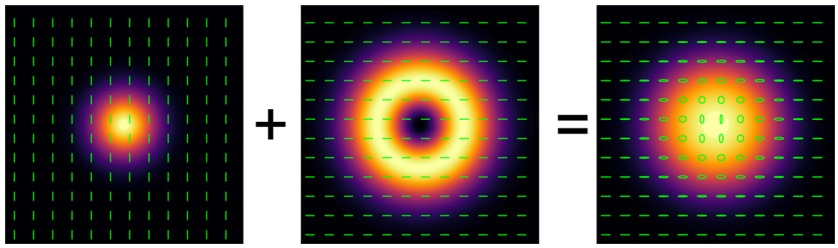

FIG. 1. Schematic of the nonuniform polarization of vector light with a Gaussian intensity profile.

are set to be immobile. The density is chosen below quarter-critical density, because the absolute modes of TPD and SRS grow near quarter-critical density, and they can compete[31] or transition,[32] or even induce further secondary instabilities.[33] The convective mode of TPD grows at a relatively low density[34] (~$0.21n_c$ to $0.245n_c$). In this simulation, the short scale length makes SRBS less important, the density range excludes the absolute mode of TPD and reduces the convectively growing length of TPD, and the immobile ions eliminate SBS. Hence, SRSS is the dominant LPI process.

The simulation region measures $34 \times 34 \times 38\ \mu m^3$, with a grid number of $340 \times 340 \times 380$. Ten particles are placed in each grid, and the total simulation time is $1000T$, where T denotes one laser period. Typically, periodic boundary conditions are used to facilitate the growth of SRSS.[7,31] However, owing to the nonperiodic polarization distribution of the vector light and to ensure consistency between these two cases, open boundaries are adopted here. Nonetheless, as we will demonstrate later, SRSS is rapidly excited in case 1 even with transverse open boundaries. Thermal boundary conditions are applied to particles.

C. Comparison between cases 1 and 2

The results for case 1 (linearly polarized Gaussian light) are shown in Figs. 3 and 4. As shown in Fig. 2, in case 1, the pump laser is polarized in the x direction, the scattered wave vector at 90° relative to the density profile is in the y direction, and thus the magnetic field of the scattered light is B_z. The electrostatic wave has wave vectors (or electric fields) $k_y(E_y)$ and $k_z(E_z)$. Figure 3 depicts the electrostatic energy integrated over z in the y–z plane, i.e., $\int |E_y(y,z)|^2 dz$, which reflects the convective growth of SRSS in the transverse direction. Since the pump is polarized in the x direction, the SRSS occurs in the y–z plane. In this configuration, the electrostatic field excited by SRSS consists of both E_y and E_z components, whereas the electrostatic field excited by SRBS has only an E_z component. As a result, the integrated electrostatic energy, which exhibits convective growth, is solely attributable to excitation by SRSS. The SRSS seed originates at the center owing to the maximum laser intensity there, and as its amplitude grows, the profile expands and takes a flat-topped form at a time of about $320T$, owing to convective saturation.

The electrostatic field and its k-space distribution in the plane where SRSS occurs (i.e., the y–z plane) and the magnetic field of the scattered light in case 1 at different times are presented in Fig. 4. The three time points we have chosen are based on the convective growth of SRSS in Fig. 3. The red arrows in Figs. 4(a), 4(d),

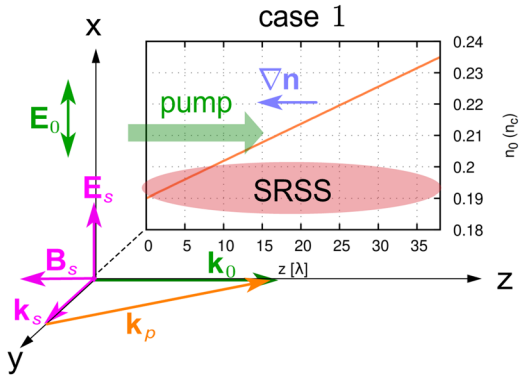

FIG. 2. Illustration of the wave vector matching relation of an x-polarized pump in SRSS and the plasma density profile. The scattered light is indicated by subscript s and magenta color, the pump light by subscript 0 and green color, and the plasma wave by subscript p and orange color.

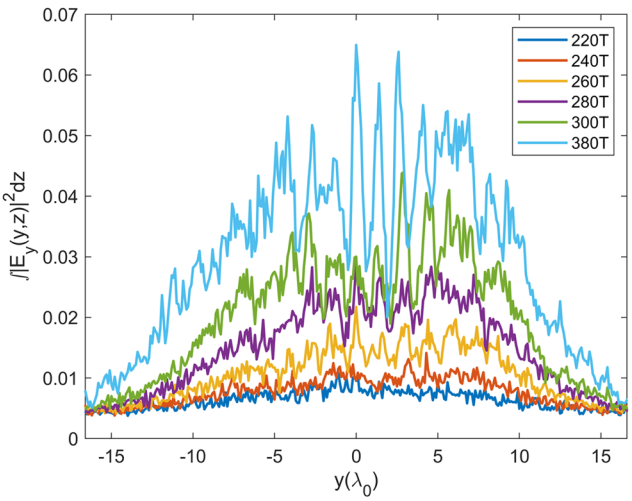

FIG. 3. Electrostatic energy $\int |E_y(y,z)|^2 dz$ in the y–$z(n_0)$ plane, integrated over the longitudinal (z) direction at different times in case 1.

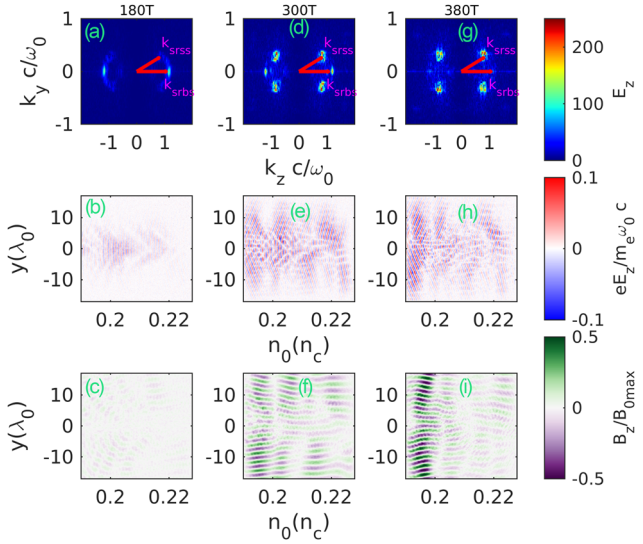

FIG. 4. Results for case 1 in the y–$z(n_0)$ plane, with x representing the direction of laser polarization perpendicular to the y–z plane shown here. SRSS occurs in the y–z plane, while SRBS occurs in the z direction. The frequency spectrum in k-space of the electrostatic field $E_z(k_y, k_z)$, the electrostatic field $E_z(y, z)$, and the magnetic field of the scattered light of SRSS $B_z(y, z)$ are plotted at times $180T$ [(a)–(c)], $300T$ [(d)–(f)], and $380T$ [(g)–(i)].

and 4(g) denote the wave vector of the electrostatic field excited by SRSS, with

$$\mathbf{k}_{\mathrm{srss}} = \left(\sqrt{1 - n/n_c},\ \sqrt{1 - 2\sqrt{n/n_c}}\right)\omega_0/c,$$

and SRBS, with

$$\mathbf{k}_{\mathrm{srbs}} = \left(\sqrt{1 - n/n_c} + \sqrt{1 - 2\sqrt{n/n_c}},\ 0\right)\omega_0/c,$$

where the plasma density is taken to be the average density $n = 0.2125n_c$. At time $180T$, the electrostatic waves are locally excited in various directions, among which the backscatter has the greatest strength owing to its higher growth rate. As the instability no longer develops locally, the intensity of SRSS is much greater than that of SRBS. At $300T$, SRSS dominates, and at $380T$, SRBS completely disappears, leaving only SRSS. Although periodic boundary conditions were not applied, SRSS has already convected transversely beyond the pump waist width.

Figures 4(c), 4(f), and 4(i) show the distribution of the magnetic field B_z of the scattered electromagnetic wave, which is normalized by the maximum magnetic field $B_{0\mathrm{max}}$ of the incident laser field. At time $300T$, the scattered light intensity is nearly uniform in the z direction, whereas at $380T$, the scattered light is stronger near the left boundary. Despite a higher growth rate in the high-density region, the incident light enters from the left, and scatters off some energy in the low-density region, which causes an intensity distribution of the scattered light in the z direction. Notably, the transverse intensity of the scattered light at $380T$ remains significant, $\sim 0.6B_{0\mathrm{max}}$, even without the implementation of periodic boundary conditions. Moreover, it is clearly seen that the scattered light presents a 90° scattering angle.

Figure 5 provides a comparison with Fig. 4 by illustrating the electrostatic wave and electromagnetic wave excited by vector light in case 2. The scattered wave vector of SRSS is not only in the y direction but in all directions in the transverse (x–y) plane. Here we choose the x–z and y–z longitudinal planes to illustrate the SRS of vector light. The wave vector spectra in the k_x–k_z and k_y–k_z planes of the electrostatic field E_z are depicted in Figs. 5(a)–5(d). Figures 5(e)–5(h) show the electrostatic field distribution E_z, and Figs. 5(j)–5(m) show the magnetic field of scattered light of SRSS, B_z, in the two longitudinal planes.

At time $200T$, in contrast to case 1, the vector light shows only a backscattering signal. At $360T$, SRBS completely disappears and SRSS survives with rather high intensity in case 1, whereas in case 2, there is still no SRSS but SRBS remains. This is because SRSS grows preferentially under the given parameters, and in case 1, the SRBS is limited by the small density length scale as well as by competition

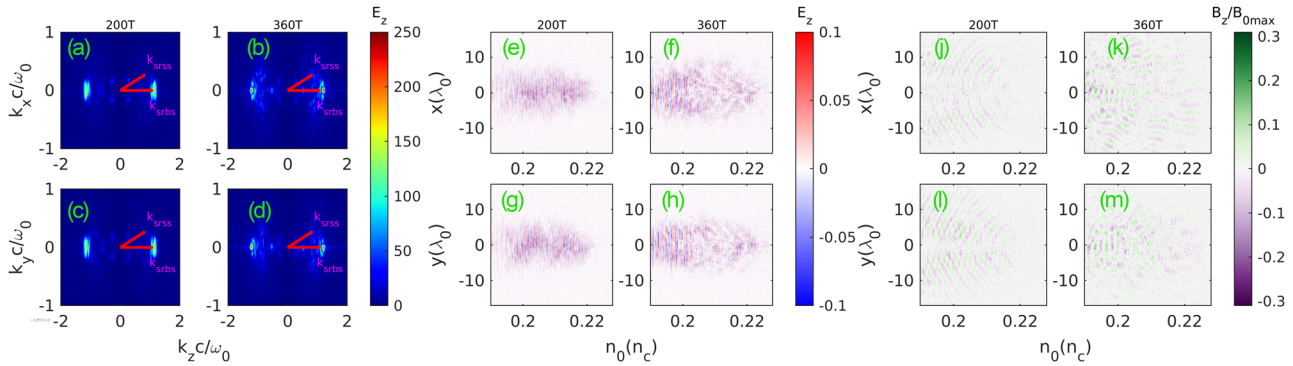

FIG. 5. Results for case 2. The frequency spectra in k-space of the electrostatic field E_z are depicted in the k_z–k_x plane [(a) and (b)] and the k_z–k_y plane [(c) and (d)], the electrostatic field distributions E_z are shown in the x–$z(n_0)$ plane [(e) and (f)] and the y–$z(n_0)$ plane [(g) and (h)], and the magnetic field distributions of the scattered light of SRSS B_z are plotted in the x–$z(n_0)$ plane [(j) and (k)] and the y–$z(n_0)$ plane [(l) and (m)], at times $200T$ and $360T$, respectively.

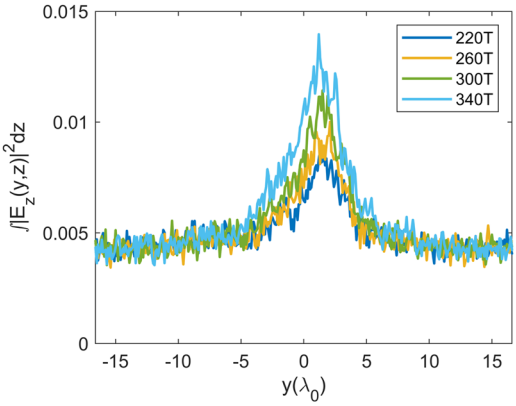

FIG. 6. Electrostatic energy $\int |E_z(y,z)|^2 dz$ in the y–z plane (perpendicular to the laser electric field), integrated over the longitudinal (z) direction at different times.

from SRSS. However, in case 2, the transverse polarization variation presents an obstacle to the development of SRSS, which reduces the competition and thus causes the SRBS to grow, but the amplitude of the EPW excited by SRBS is still lower than that excited by SRSS in case 1. Furthermore, Figs. 5(e)–5(h) demonstrate that the width of the electrostatic wave distribution is restricted within the beam waist.

The magnetic field of the backscattered light lies in the x–y plane, and only the side-scattered signal is presented in Figs. 5(j)–5(m). From B_z, we can distinguish a weak SRSS at time $200T$. At $360T$, the intensity of the scattered electromagnetic wave is still weak. Furthermore, at $360T$, the scattering occurs in all directions, rather than at the angle of 90° in case 1. This is also in line with our starting point and indicates that the change in direction of polarization can cause the wave vector of the scattered light to change, thereby preventing the SRSS from transverse convection.

Figure 6 depicts the electrostatic energy $\int |E_z(y,z)|^2 dz$ in the y–z plane (perpendicular to the laser electric field), integrated over the longitudinal (z) direction at different times. The electrostatic field excited by SRBS is E_z. For a quantitative comparison with the electrostatic energy induced by SRSS in case 1, we integrate the energy over the z direction in the y–z plane. Notably, in case 2, both the intensity and the total energy of the electrostatic field induced by SRBS are significantly lower than those in case 1. This emphasizes that, for the same parameter configuration, the suppression of SRSS by vector light does not lead to an enhancement of SRBS. Additionally, in contrast to Fig. 3, Fig. 6 clearly demonstrates the absolute growth of SRBS.

III. ANALYSIS

The suppressive effect of vector light on SRSS has been demonstrated in Sec. II. In this section, a parametric discussion about vector light to inhibit SRSS is presented.

The theory of SRSS[6,35] has been reviewed in Ref. 7. Two approaches have been developed to describe the growth of SRSS: the wave packet solution and eigenmode theory.[7,35] The minimum saturation time t_s of the convective mode is used as the criterion to identify whether convective or absolute growth dominates. If the growth time t is less than $2t_s$, wave packet (convective growth) dominates, and it has a finite exponential gain owing to the refraction of scattered light in a nonuniform plasma. The minimum saturation time is[7]

$$t_s \approx 8.5\left(\frac{\omega_0-\omega_p}{\omega_p}\right)^{1/2}\left(\frac{k_p v_0}{\omega_p}\right)^{1/2}\frac{L_n}{c}, \tag{2}$$

where ω_p and ω_0 are the plasma frequency and laser frequency, v_0 and c are the electron quiver velocity in the laser field and the speed of light, respectively, k_p is the wave vector of the EPW, and L_n is the density scale length. After $t > 2t_s$, the eigenmode (absolute growth) dominates, and the growth rate can be found in Ref. 7. The threshold parameter is given by[7]

$$\eta_a = \left(\frac{v_0}{c}\right)^{1/2}\left(\frac{\omega_0 L_n}{c}\right)^{4/3}\frac{2-2\omega_p/\omega_0-\omega_p^2/\omega_0^2}{(\omega_p/\omega_0)^{2/3}}, \tag{3}$$

and the threshold is $\eta_a = 1$.

Under the conditions of the simulation cases 1 and 2, the threshold η_a is 58, which far exceeds the threshold. Therefore, the threshold condition is only appropriate for a pump with uniform polarization. Once there is a polarization distribution over the cross-section of the pump beam, an additional threshold defined by the characteristic length of polarization variation L_p is requisite. Under the assumption that the polarization of the initial scattered seed excited at a certain location is aligned with the polarization of the pump locally, as the scattered light convects out of the resonant location, the electric field of the pump will not be collinear with the seed. Consequently, the seed cannot be amplified further, and the excited EPW will be damped finally owing to Landau and/or collisional damping. The condition for the seed to be able to grow continuously is that the growth distance L before saturation is much less than L_p, i.e.,

$$L = 2V_{ge}t_s < L_p, \tag{4}$$

where $V_{ge} = (V_s + V_e)/2 \approx V_s/2$ is the effective group velocity,[6] $V_e = 3v_e^2 k_\perp/\omega_p$ and $V_s = c^2 k_s/(\omega_0-\omega_p)$ are the group velocities of the electrostatic wave and scattered electromagnetic wave, respectively, $k_\perp$ is the perpendicular wave vector of the electrostatic wave, v_e is the thermal velocity of electrons, and k_s is the wave vector of the scattered light. Substituting the saturation time gives the threshold condition defined by L_p:

$$8.5\left(\frac{k_p v_0}{\omega_0-\omega_p}\right)^{1/2} L_n \frac{ck_s}{\omega_p} < L_p. \tag{5}$$

For normally incident pump light, the threshold condition is

$$L_{p,\min}^2 = 0.616\sqrt{I_{14}}\,\lambda_{\mu m} L_n^2 \frac{\left(1-\frac{2\omega_p}{\omega_0}\right)\sqrt{2-\frac{2\omega_p}{\omega_0}-\frac{\omega_p^2}{\omega_0^2}}}{(1-\omega_p\omega_0)\omega_p^2\omega_0^2}, \tag{6}$$

where I_{14} denotes the laser intensity in units of 10^{14} W/cm^2, $\lambda_{\mu m}$ is the wavelength of the pump light in micrometers, and $L_{p,\min}$ is the minimum characteristic length of polarization variation to trigger SRSS after other parameters have been given. Taking

typical parameters of an ICF experiment on the NIF[13] as an example, namely, $I_{14} = 8$, $\lambda_{\mu m} = 0.351$, $L_n = 500\ \mu$m, and $\omega_p/\omega_0 = 0.44$, where the density is about 0.2 times the critical density, the minimum characteristic length of polarization is about $0.5L_n$, which means that SRSS can be inhibited if $L_p < 0.5L_n$, even when the $\eta_a = 4.6$ exceeds the threshold.

IV. DISCUSSION

As shown by the simulations and analysis, the transversely nonuniform polarization distribution of the vector light contributes to the suppression of the convective growth of SRSS, which has transverse propagation and growth. It is straightforward to conjecture that this transversely nonuniform polarization has little effect on the longitudinally propagating SRBS. As is also evidenced in Fig. 5, the polarization distribution can suppress transverse convection, but cannot inhibit the backscattering. With regard to TPD, considering that the wave vectors of the two daughter EPWs possess transverse components, there is also an effective damping rate due to polarization change as $\nu = V_{ge}/L_p$, where $V_{ge} = V_e = 3v_e^2 k_\perp/\omega_p$. For a rough estimation, taking the plasma parameters to be $T_e = 2000$ eV, $L_p = 15\lambda_0$, $n_0 = 0.25n_c$, $k_\perp = 0.1\omega_0/c$, $I_0 = 5.0 \times 10^{14}$ W/cm^2, and $\lambda = 0.351\ \mu$m (typical of ICF experiments on OMEGA), the effective damping rate is $\nu \sim 10^{-5}\omega_0$. For these parameters, the growth rate of TPD is about $10^{-3}\omega_0$. Thus, the effective damping caused by the nonuniform polarization seems insignificant compared with the growth rate. Thus, the suppressive effect of the transverse polarization distribution on TPD is negligible, because the group velocity of EPWs is so small that the polarization change cannot be experienced during the growth time of instability.

Although the suppression scheme based on vector light described here is aimed at SRSS driven by a single-beam laser pump, it is also applicable to the stimulated Brillouin side-scattering (SBSS) driven by a single-beam or multibeam pump that has been observed experimentally.[36] Previous research has shown that when the directions of polarization of the two pump beams are orthogonal, the gain coefficient of collective SBSS decreases to the level of single-beam side-scattering.[37] To effectively suppress collective SBS, we propose to design pump vector lights with orthogonal polarization distributions, thereby preventing the occurrence of collective SBS while allowing for single-beam SBS side-scattering. Further, the amplification length of single-beam Brillouin side-scattering is reduced from w_b (the width of the pump beams) to L_p, which can decrease the gain. Thus, adjusting the polarization distributions of both pump beams enables suppression of both single-beam SBSS and collective SBS.

In this study, we have proposed a method to suppress SRSS using vector light, which can inhibit the convective growth of SRSS and prevent it from entering the absolute mode stage. We have confirmed the effectiveness of this approach through 3D PIC simulations. Our simulation results show that linearly polarized Gaussian light generates a strong SRSS signal in the 90° direction, whereas vector light generates few SRSS signals, even when the conditions far exceed the threshold for SRSS. We have also established a threshold condition based on the characteristic length of variation of polarization. This work is the first to explore the inhibition of LPI from the perspective of the vector nature of the light field, offering a new possibility for suppressing LPI and paving the way for future research.

ACKNOWLEDGMENTS

This research was supported by the Strategic Priority Research Program of the Chinese Academy of Sciences under Grant Nos. XDA25050400 and XDA25010200, and by the National Natural Science Foundation of China (NSFC) under Grant Nos. 12175229 and 11975014.

AUTHOR DECLARATIONS

Conflict of Interest

The authors have no conflicts to disclose.

Author Contributions

Xiaobao Jia: Conceptualization (equal); Data curation (equal); Formal analysis (equal); Investigation (equal); Methodology (equal); Software (equal); Validation (equal); Visualization (equal); Writing – original draft (equal). **Qing Jia**: Conceptualization (equal); Formal analysis (equal); Funding acquisition (equal); Project administration (equal); Resources (equal); Software (equal); Supervision (equal); Writing – review & editing (equal). **Rui Yan**: Formal analysis (equal); Funding acquisition (equal); Methodology (equal); Resources (equal); Software (equal); Supervision (equal); Validation (equal); Writing – review & editing (equal). **Jian Zheng**: Conceptualization (equal); Formal analysis (equal); Funding acquisition (equal); Methodology (equal); Project administration (equal); Resources (equal); Supervision (equal); Validation (equal); Writing – review & editing (equal).

DATA AVAILABILITY

The data that support the findings of this study are available from the corresponding author upon reasonable request.

APPENDIX: THE INTENSITY DISTRIBUTION OF THE PUMP LASERS IN CASE 1 AND CASE 2

The transverse intensity distribution of the pump lasers of case 1 and case 2 are presented in Fig. 7. It is worth noting that the power of the vector light is slightly higher in the high-intensity

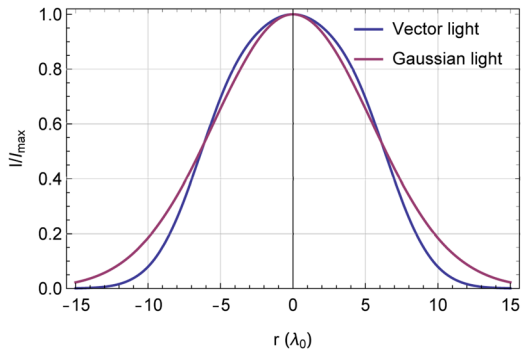

FIG. 7. Comparison of the intensity distribution of the pump in case 1 (linearly polarized Gaussian light) and case 2 (vector light).

region (central region) compared with that of the Gaussian light. Conversely, the Gaussian light exhibits more power distributed in the low-intensity region (marginal region). Although the total powers of the two cases differ slightly, specifically 12.69 (arbitrary units) of case 1 vs 13.55 of case 2, the powers in the central region where the intensity exceeds the threshold for SRSS ($I > 3.16 \times 10^{14}$ W/cm^2) are nearly the same, with values of 12.49 in case 1 vs 12.73 in case 2. Thus, the difference in power distributed in the marginal region has little effect.

REFERENCES

[1]D. W. Forslund, J. M. Kindel, and E. L. Lindman, "Theory of stimulated scattering processes in laser-irradiated plasmas," Phys. Fluids **18**, 1002 (1975).

[2]C. S. Liu, M. N. Rosenbluth, and R. B. White, "Raman and Brillouin scattering of electromagnetic waves in inhomogeneous plasmas," Phys. Fluids **17**, 1211 (1974).

[3]J. F. Myatt, J. Zhang, R. W. Short, A. V. Maximov, W. Seka, D. H. Froula, D. H. Edgell, D. T. Michel, I. V. Igumenshchev, D. E. Hinkel, P. Michel, and J. D. Moody, "Multiple-beam laser–plasma interactions in inertial confinement fusion," Phys. Plasmas **21**, 055501 (2014).

[4]W. L. Kruer, S. C. Wilks, B. B. Afeyan, and R. K. Kirkwood, "Energy transfer between crossing laser beams," Phys. Plasmas **3**, 382–385 (1996).

[5]C. J. McKinstrie, J. S. Li, R. E. Giacone, and H. X. Vu, "Two-dimensional analysis of the power transfer between crossed laser beams," Phys. Plasmas **3**, 2686–2692 (1996).

[6]M. A. Mostrom and A. N. Kaufman, "Raman side-scatter instability in nonuniform plasma," Phys. Rev. Lett. **42**, 644–647 (1979).

[7]C. Z. Xiao, H. B. Zhuo, Y. Yin, Z. J. Liu, C. Y. Zheng, Y. Zhao, and X. T. He, "On the stimulated Raman sidescattering in inhomogeneous plasmas: Revisit of linear theory and three-dimensional particle-in-cell simulations," Plasma Phys. Controlled Fusion **60**, 025020 (2018).

[8]P. Michel, L. Divol, E. L. Dewald, J. L. Milovich, M. Hohenberger, O. S. Jones, L. B. Hopkins, R. L. Berger, W. L. Kruer, and J. D. Moody, "Multibeam stimulated Raman scattering in inertial confinement fusion conditions," Phys. Rev. Lett. **115**, 055003 (2015).

[9]E. L. Dewald, F. Hartemann, P. Michel, J. Milovich, M. Hohenberger, A. Pak, O. L. Landen, L. Divol, H. F. Robey, O. A. Hurricane, T. Döppner, F. Albert, B. Bachmann, N. B. Meezan, A. J. MacKinnon, D. Callahan, and M. J. Edwards, "Generation and beaming of early hot electrons onto the capsule in laser-driven ignition hohlraums," Phys. Rev. Lett. **116**, 075003 (2016).

[10]R. S. Craxton, K. S. Anderson, T. R. Boehly, V. N. Goncharov, D. R. Harding, J. P. Knauer, R. L. McCrory, P. W. McKenty, D. D. Meyerhofer, J. F. Myatt, A. J. Schmitt, J. D. Sethian, R. W. Short, S. Skupsky, W. Theobald, W. L. Kruer, K. Tanaka, R. Betti, T. J. B. Collins, J. A. Delettrez, S. X. Hu, J. A. Marozas, A. V. Maximov, D. T. Michel, P. B. Radha, S. P. Regan, T. C. Sangster, W. Seka, A. A. Solodov, J. M. Soures, C. Stoeckl, and J. D. Zuegel, "Direct-drive inertial confinement fusion: A review," Phys. Plasmas **22**, 110501 (2015).

[11]R. Betti, C. D. Zhou, K. S. Anderson, L. J. Perkins, W. Theobald, and A. A. Solodov, "Shock ignition of thermonuclear fuel with high areal density," Phys. Rev. Lett. **98**, 155001 (2007).

[12]S. Depierreux, C. Neuville, C. Baccou, V. Tassin, M. Casanova, P.-E. Masson-Laborde, N. Borisenko, A. Orekhov, A. Colaitis, A. Debayle, G. Duchateau, A. Heron, S. Huller, P. Loiseau, P. Nicolaï, D. Pesme, C. Riconda, G. Tran, R. Bahr, J. Katz, C. Stoeckl, W. Seka, V. Tikhonchuk, and C. Labaune, "Experimental investigation of the collective Raman scattering of multiple laser beams in inhomogeneous plasmas," Phys. Rev. Lett. **117**, 235002 (2016).

[13]M. J. Rosenberg, A. A. Solodov, J. F. Myatt, W. Seka, P. Michel, M. Hohenberger, R. W. Short, R. Epstein, S. P. Regan, E. M. Campbell, T. Chapman, C. Goyon, J. E. Ralph, M. A. Barrios, J. D. Moody, and J. W. Bates, "Origins and scaling of hot-electron preheat in ignition-scale direct-drive inertial confinement fusion experiments," Phys. Rev. Lett. **120**, 055001 (2018).

[14]P. Michel, M. J. Rosenberg, W. Seka, A. A. Solodov, R. W. Short, T. Chapman, C. Goyon, N. Lemos, M. Hohenberger, J. D. Moody, S. P. Regan, and J. F. Myatt, "Theory and measurements of convective Raman side scatter in inertial confinement fusion experiments," Phys. Rev. E **99**, 033203 (2019).

[15]G. Cristoforetti, L. Antonelli, D. Mancelli, S. Atzeni, F. Baffigi, F. Barbato, D. Batani, G. Boutoux, F. D'Amato, and J. Dostal, "Time evolution of stimulated Raman scattering and two-plasmon decay at laser intensities relevant for shock ignition in a hot plasma," High Power Laser Sci. Eng. **7**, e51 (2019).

[16]K. Glize, X. Zhao, Y. Zhang, C. Lian, S. Tan, F. Wu, C. Xiao, R. Yan, Z. Zhang, X. Yuan, and J. Zhang, "Measurement of stimulated Raman side-scattering predominance in directly driven experiment," Proc. Nat. Acad. Sci. U.S.A. (submitted); arXiv.2209.08251 [physics] (2023).

[17]J. Zhang, W. M. Wang, X. H. Yang, D. Wu, Y. Y. Ma, J. L. Jiao, Z. Zhang, F. Y. Wu, X. H. Yuan, Y. T. Li, and J. Q. Zhu, "Double-cone ignition scheme for inertial confinement fusion," Philos. Trans. R. Soc., A **378**, 20200015 (2020).

[18]C. Rosales-Guzmán, B. Ndagano, and A. Forbes, "A review of complex vector light fields and their applications," J. Opt. **20**, 123001 (2018).

[19]Q. Zhan, "Cylindrical vector beams: From mathematical concepts to applications," Adv. Opt. Photonics **1**, 1 (2009).

[20]X.-L. Wang, J. Ding, W.-J. Ni, C.-S. Guo, and H.-T. Wang, "Generation of arbitrary vector beams with a spatial light modulator and a common path interferometric arrangement," Opt. Lett. **32**, 3549–3551 (2007).

[21]H. T. Wang, X. L. Wang, Y. Li, J. Chen, C. S. Guo, and J. Ding, "A new type of vector fields with hybrid states of polarization," Opt. Express **18**, 10786–10795 (2010).

[22]R. K. Follett, J. G. Shaw, J. F. Myatt, C. Dorrer, D. H. Froula, and J. P. Palastro, "Thresholds of absolute instabilities driven by a broadband laser," Phys. Plasmas **26**, 062111 (2019).

[23]Y. Zhao, C. F. Wu, S. Weng, Z. Sheng, and J. Zhu, "Mitigation of multibeam stimulated Raman scattering with polychromatic light," Plasma Phys. Controlled Fusion **63**, 055006 (2021).

[24]H. H. Ma, X. F. Li, S. M. Weng, S. H. Yew, S. Kawata, P. Gibbon, Z. M. Sheng, and J. Zhang, "Mitigating parametric instabilities in plasmas by sunlight-like lasers," Matter Radiat. Extremes **6**, 055902 (2021).

[25]D. H. Munro, S. N. Dixit, A. B. Langdon, and J. R. Murray, "Polarization smoothing in a convergent beam," Appl. Opt. **43**, 6639–6647 (2004).

[26]S. Skupsky, R. W. Short, T. Kessler, R. S. Craxton, S. Letzring, and J. M. Soures, "Improved laser-beam uniformity using the angular dispersion of frequency-modulated light," J. Appl. Phys **66**, 3456–3462 (1989).

[27]I. Barth and N. J. Fisch, "Reducing parametric backscattering by polarization rotation," Phys. Plasmas **23**, 102106 (2016).

[28]T. D. Arber, K. Bennett, C. S. Brady, A. Lawrence-Douglas, M. G. Ramsay, N. J. Sircombe, P. Gillies, R. G. Evans, H. Schmitz, A. R. Bell, and C. P. Ridgers, "Contemporary particle-in-cell approach to laser-plasma modelling," Plasma Phys. Controlled Fusion **57**, 113001 (2015).

[29]T. Bauer, P. Banzer, E. Karimi, S. Orlov, A. Rubano, L. Marrucci, E. Santamato, R. W. Boyd, and G. Leuchs, "Observation of optical polarization Möbius strips," Science **347**, 964–966 (2015).

[30]M. J. Padgett, "Orbital angular momentum 25 years on [invited]," Opt. Express **25**(10), 11265–11274 (2017).

[31]H. Wen, A. V. Maximov, R. Yan, J. Li, C. Ren, and F. S. Tsung, "Three-dimensional particle-in-cell modeling of parametric instabilities near the quarter-critical density in plasmas," Phys. Rev. E **100**, 041201 (2019).

[32]C. Xiao, H. Zhuo, Y. Yin, Z. Liu, C. Zheng, and X. He, "Transition from two-plasmon decay to stimulated Raman scattering under ignition conditions," Nucl. Fusion **60**, 016022 (2020).

[33]K. Q. Pan, S. E. Jiang, Q. Wang, L. Guo, S. W. Li, Z. C. Li, D. Yang, C. Y. Zheng, B. H. Zhang, and X. T. He, "Two-plasmon decay instability of the backscattered light of stimulated Raman scattering," Nucl. Fusion **58**, 096035 (2018).

[34]R. Yan, A. V. Maximov, and C. Ren, "The linear regime of the two-plasmon decay instability in inhomogeneous plasmas," Phys. Plasmas **17**, 052701 (2010).

[35]B. B. Afeyan and E. A. Williams, "Stimulated Raman sidescattering with the effects of oblique incidence," Phys. Fluids **28**, 3397 (1985).

[36]D. Turnbull, P. Michel, J. E. Ralph, L. Divol, J. S. Ross, L. F. Berzak Hopkins, A. L. Kritcher, D. E. Hinkel, and J. D. Moody, "Multibeam seeded Brillouin sidescatter in inertial confinement fusion experiments," Phys. Rev. Lett. **114**, 125001 (2015).

[37]J. Qiu, L. Hao, L. Cao, and S. Zou, "Collective stimulated Brillouin scattering modes of two crossing laser beams with shared scattered wave," Matter Radiat. Extremes **6**, 065903 (2021).